RSC Advances

ROYAL SOCIETY OF CHEMISTRY

www.rsc.org/advances

Atmospheric chemistry of alkyl iodides: theoretical studies on the mechanisms and kinetics of $CH_3I/C_2H_5I + NO_3$ reactions

Feng-Yang Bai, Xu Wang, Yan-Qiu Sun, and Xiu-Mei Pan*

Institute of Functional Material Chemistry, Faculty of Chemistry, Northeast Normal University, Changchun, 130024 People's Republic of China

Abstract

The gas-phase reactions of CH_3I and C_2H_5I with NO_3 radical are studied by the dual-level direct kinetics method. The minimum energy paths are refined by CCSD(T) and QCISD(T) methods. One displacement and two hydrogen abstraction processes are found for reaction $CH_3I + NO_3$. For reaction of $C_2H_5I + NO_3$, three hydrogen abstraction and one displacement channels are found. The hydrogen abstraction from $-CH_2-$ group is found to be the dominant channel. The displacement channel of the title reactions may be negligible because of the high barrier. The rate constants for the individual reaction channels are followed by means of canonical variational transition state with the small-curvature tunneling correction. Calculated rate constants are in reasonable agreement with the available data in experiment. The Arrhenius expressions for the title reactions are given as follows: $k_a=8.62\times10^{-32}T^{6.66}\exp(1324.23/T)$, $k_b=9.48\times10^{-27}T^{5.75}\exp(-655.34/T)$ cm^3 $molecule^{-1}$ s^{-1}. The atmospheric lifetime of CH_3I and C_2H_5I determined by NO_3 radical is about 3.07 and 5.86 h, which indicates that they can be degraded in the gas phase within short time as a source of reactive iodine compounds at nighttime.

Keywords: Transition state, Hydrogen abstraction, Rate constant, Atmospheric lifetime

* Author to whom correspondence should be addressed. Electronic addresses: panxm460@nenu.edu.cn and ftao@fullerton.edu.

1. Introduction

Organic halogenides release into the atmosphere is caused to the largest extent by micro and macro algae metabolism in the open oceans and sea coastal regions.[1] The key iodine-containing volatile organic compounds (IVOCs), methyl iodide (CH_3I), diiodomethane (CH_2I_2), iodoethane (C_2H_5I), 1-iodopropane (n-C_3H_7I), and 2-iodopropane (iso-C_3H_7I) are being of central importance in understanding iodine chemistry in the marine boundary layer. They play significant roles in ozone destruction by reaction with O_3 to form IO radical, resulting in the changed oxidation capacity of the atmosphere[2,3] and also contribute to the tropospheric iodine budget.[4-6] The halogenated organic species can be removed by photo dissociation processes upon the formation of atomic halogens and can also react with OH, Cl during the day and NO_3 at night in the atmosphere.[1,7,8] Note that some IVOCs reaction with NO_3 radical would play an important role in the atmospheric iodine cycle at nighttime.[9-12]

NO_3 radicals are important oxidant in the atmosphere at night. Its reactivity is comparable to that of OH radicals in the atmosphere.[13] The abundance of NO_x in the troposphere can lead to the formation of the nitrate radical NO_3 by the following reactions:

$$NO + O_3 \rightarrow NO_2 + O_2 \quad (1)$$

$$NO_2 + O_3 \rightarrow NO_3 + O_2 \quad (2)$$

The NO_3 concentration remains low during daylight because it can be rapidly photolyzed.[14] However, it can increase to reach measurable levels at nighttime. Some measurements at ground level have yielded nighttime NO_3 average concentrations[15,16] of 5×10^8 to 2×10^9 molecule cm^3. On account of its high concentration at night, NO_3 radicals may play an important role in controlling the lifetimes of atmospheric IVOCs.

In addition, the NO_3 radical contributes to the oxidation of alkanes and to the formation of HNO_3, which is also related to particulate formation and harmful health effects.[17] In the last years, attention has been taken to the NO_3 nighttime reactivity in urban zones with a series of hydrogen compounds.[18-22] Here, we will focus on the important iodine cycle reactions, CH_3I and C_2H_5I with NO_3 radicals. The reactions can proceed via seven reactions channels including H-abstraction (R1a, R2a, R1b, R2b, R3b) and displacement (R3a, R4b), e.g.,

$CH_3I + NO_3 \rightarrow CH_2I + HNO_3$ (R1a, R2a)

$CH_3I + NO_3 \rightarrow CH_3NO_3 + I$ (R3a)

$C_2H_5I + NO_3 \rightarrow CH_3CHI + HNO_3$ (R1b)

$C_2H_5I + NO_3 \rightarrow CH_2CH_2I + HNO_3$ (R2b, R3b)

$C_2H_5I + NO_3 \rightarrow CH_3CH_2NO_3 + I$ (R4b)

Reactions of NO_3 with CH_3I and C_2H_5I were reported by Nakano et al.[9,12] through the cavity ring-down spectroscopy method. The rate constant was determined to be $(4.1 \pm 0.2) \times 10^{-13}$ for reaction $CH_3I + NO_3$, and $(2.4 \pm 0.4) \times 10^{-13}$ cm^3 $molecule^{-1}$ s^{-1} for reaction $C_2H_5I + NO_3$ at 298 K. In order to enrich the rate constants of reaction NO_3 with CH_3I, Nakano et al.[11] have also used same method to obtain the rate constants at the temperature range of 298−323 K. They also calculated the minimum energy paths (MEPs) by Density Functional and Coupled-Cluster calculations. The results obtained by them are in good line with our results. The experimental Arrhenus expression was determined to be $k_{CH_3I+NO_3} = 9.1^{+18.4}_{-6.10} \times 10^{-11} \exp[(-1600 \pm 300)/T]$. However, the experiment and theory did not cover a wide temperature range of practical interest. Thus, theoretical studies on the accurate extrapolation of rate constants in wide temperature range for the title reactions are very necessary. Nakano

et al.[9,12] have estimated the lifetime of CH_3I and C_2H_5I is 3 and 5 hours in experiment, respectively. But until now the lifetime of CH_3I and C_2H_5I is still unknown in theory. The atmospheric lifetime of CH_3I and C_2H_5I is such a great significance to the understanding of their environmental behaviors and potential impacts on human health and iodine cycle at night that needing to be estimated. The reaction mechanisms and the dynamics content are also needed to give a further understanding.

As far as we know, no other experimental and theoretical researches have been reported. In this study, B3LYP, CCSD(T), and QCISD(T) calculations are performed on the reaction mechanisms of the title reactions. A dual-level direct dynamics studies for the rate constants over a wide temperature region of 220–800 K was used. The rate constants, which used to obtain the parameters for the modified Arrheius equation and product branching ratios are calculated by the variational transition state theory (VTST) with interpolated single-point energies (ISPE). The lifetime of CH_3I and C_2H_5I is also estimated. The experimental and computational results are discussed as well as the branching ratios of the title reactions.

2. Computational details

The electronic structure calculations are carried out with Gaussian 09 program package.[23] The equilibrium geometries of the reactants, products, complexes, and transition states are optimized at the Becke's three parameter hybrid functional with then on local correlation functional of Lee–Yang–Par level (B3LYP) of theory[24,25] using the standard 6-311++G(d,p) basis set for C, H, N, O and cc-pVTZ-PP[26] basis set for iodine. The cc-pVTZ-PP basis set includes an effective-core-potential (ECP) for

iodine to decrease the cost of computation and describe the relativistic effects. The basis sets are together called as basis set I. Harmonic vibrational frequencies calculations were performed at the same level of theory in order to determine the nature of the various stationary points, as well as zero-point energy (ZPE) corrections. The B3LYP method was proven to be an economic and accurate computational model for predicting electronic structure in many articles.[27,28] The transition states were verified by the intrinsic reaction coordinate (IRC)[29,30] calculations to connect the designated reactants and products. In order to obtain more reliable relative energy of each stationary point on the potential energy surfaces (PES), single point energy calculations have been performed by the higher level methods CCSD(T)[31] and QCISD(T).[32] The basis sets of aug-cc-pVTZ-PP[33] and 6-311++G(d,p) for iodine atom and the remaining atoms were employed, respectively. The aug-cc-pVTZ-PP basis set also includes an effective-core-potential (ECP) for iodine. The above combined basis sets are defined as basis set II. The T_1–diagnostic is a qualitative measure of multireference character. The T_1 values of all species in our system are smaller than 0.045, indicating that multireference character in CCSD(T) wave functions is not a problem.[34,35]

On the basis of the initial PES information, including optimized geometries, energies, and frequencies along the MEPs, the rate constants are calculated over the wide temperature range of 220–800 K using the canonical variational transition state theory (CVT)[36-38] involving small curvature tunneling correction (SCT)[39,40] method proposed by Truhlar and co-workers. The dynamic calculations of the variational

transition state theory with interpolated single-point energies (VTST-ISPE)[41] are carried out through the POLYRATE-Version 9.7 program.[42]

As is well we known that the severe spin contamination can lead to imprecise values in the barrier height.[43,44] Thus, the spin contamination are examined before and after annihilation for the species related to the title reactions. The doublet range from 0.752 to 0.777 before annihilation, nevertheless, the $<s^2>$ is 0.75 (the exact data for a pure doublet) after annihilation. The wave functions were not severely contaminated by states of higher multiplicity.

3. Results and discussions

3.1 Electronic Structures of Stationary Points

The optimized structural parameters of the reactants, products, complexes, and transition states are listed in Figure 1. Figure 1 shows that the breaking C−H bond in TS1a and TS2a is 1.284 Å and 1.307 Å, which is 18.3% and 20.5% longer than the equilibrium C−H bond in CH_3I, respectively. The breaking C−I bond is elongated by 16.0% in TS3a than the equilibrium C−I bond length in CH_3I. The forming O−H (C−O) bonds are elongated by 31.1%, 29.3%, and 39.4% as compared to the O−H (C−O) equilibrium bond length of HNO_3 (CH_3NO_3), respectively. In TS1b, TS2b, and TS3b, the breaking C−H bonds are 15.9%, 13.8%, and 16.1% longer than the equilibrium C−H bond length in C_2H_5I. The forming O−H bonds are elongated by about 35.4%, 38.9%, and 33.3% compared to the regular O−H bond length. For the displacement process of reaction C_2H_5I with NO_3, the breaking C−I bond is stretched by 18.7%

compared with the C–I equilibrium bond length in C_2H_5I, whereas the forming C–O bond is about 43.1% longer than the regular bond length of the isolated $CH_3CH_2NO_3$. The elongation of the breaking bond is smaller than that of the forming bond, indicating that the transition states are reactant-like and the seven reaction processes (R1a–R4b) may proceed via early transition states. Consequently, all the seven transition states can be considered as early barriers.

The harmonic vibrational frequencies are calculated to confirm the stationary nature and to make zero-point energy (ZPE) corrections. The calculated frequencies at the B3LYP/I level are displayed in Table S1. All the reactants, products, complexes are confirmed with only real frequencies, which indicate a minimum has been located, and for each transition state yields, there is only one imaginary frequency corresponding to the stretching modes of the coupling breaking and forming bonds. The values of those imaginary frequencies are 1428*i*, 1536*i*, 683*i*, 1193*i*, 1072*i*, 1370*i*, and 536*i* cm^{-1} for TS1a, TS2a, TS3a, TS1b, TS2b, TS3b, and TS4b, respectively. These large absolute values of the imaginary frequencies for H-abstraction reactions indicate that the width of the potential barrier might be narrower and the tunneling effect may be more important in the calculation of the rate constants.

3.2 Reaction mechanisms

The schematic potential energy diagram of the title reactions with ZPE corrections, obtained at the CCSD(T)/II//B3LYP/I level, is plotted in Figure 2a and 2b. The total energies of the reactants are set at zero as a reference for other species. For reactions

R1a, R2a, and R3a, the barrier heights are 10.54, 10.33, and 23.00 kcal/mol, respectively. The barrier height of reactions R1a and R2a is very close with 0.21 kcal/mol difference in energy, indicating that the rate constant of them will compete with each other. There are three complexes, EP1a, EP2a, and EP3a, which are about –2.97, –3.43, and –19.49 kcal/mol lower than the reactants. For the reaction of C_2H_5I + NO_3, the NO_3 can abstract H atom of the $–CH_2–$ group reaction (R1b), the in-plane H atoms of the $–CH_3$ group reaction (R2b), one of the out-of-plane H atom of the $–CH_3$ group reaction (R3b), and attack the C atom of group $–CH_2–$ (R4b). Figure 2b shows that the four complexes (EP1b, EP2b, EP3b, and EP4b) in the in the exit routes, are formed through TS1b, TS2b, TS3b, and TS4b with 7.15, 9.58, 10.41, and 20.02 kcal/mol barrier heights, respectively. For reaction C_2H_5I + NO_3, we can see that R1b is the dominant reaction channel. The secondary reaction pathways R2b and R3b are nearly with 0.83 kcal/mol difference in barrier height, illustrating that the status for R2b and R3b is similar and their rate constant will compete with each other. One step further, we also find that the barrier heights of displacement reactions R3a and R4b are about 23.00 and 20.00 kcal/mol, respectively, which are higher than the H-abstraction barrier heights. Thus, the hydrogen abstraction reaction pathways are the main reaction channels and the displacement processes may be negligible. Similar conclusion can be found about reaction C_2H_5I + Cl.[45]

To understand thoroughly the kinetics and mechanism of these reactions, particularly in atmospheric modeling, accurate thermodynamic values are necessary. The relative energies (*E*r) of main species for title reactions with zero-point energy

(ZPE) corrections, reaction enthalpies ($\Delta H^{\theta}_{r,298}$), reaction Gibbs free energies ($\Delta G^{\theta}_{r,298}$) for the reactions R1a-R4b calculated at the B3LYP/I, CCSD(T)/II//B3LYP/I, and QCISD(T)/II//B3LYP/I levels, are displayed in Table 1. As shown in Table 1, the results obtained at the B3LYP, CCSD(T), and QCISD(T) levels show good mutual agreement. At the CCSD(T)/II//B3LYP/I level, it is easy from the $\Delta H^{\theta}_{r,298}$ values that all of the individual reactions are exothermic reactions. The $\Delta G^{\theta}_{r,298}$ results indicate that the hydrogen abstraction reactions of CH_3I and C_2H_5I by NO_3 radical are spontaneous. The heat of exothermic displacement reactions R3a and R4b, -18.82 and -21.20, are more than that of the H-abstraction reactions. The spontaneous tendency of the displacement reactions is also larger than the H-abstraction reactions. The value of $\Delta H^{\theta}_{r,298}$ for the H-abstraction reaction R1b, -2.67 kcal/mol, is higher than that of R2b (R3b), -7.53 kcal/mol. Comparing the $\Delta G^{\theta}_{r,298}$ value of R1b with R2b (R3b), we can find that the spontaneous tendency of former is smaller than that of the latter. Although the barrier heights of displacement reactions are hard to overcome, the corresponding products are the most stable than other.

3.3 Reaction Path Properties

The minimum energy paths are obtained by IRC calculations at the B3LYP/I level. The dual-level direct kinetics calculations are carried out to compute the dynamic content at the CCSD(T)/II//B3LYP/I level. Figure S1a and S1b depict the classical potential energy curve (V_{MEP}), ground-state vibrational adiabatic energy curve (V_a^G), and zero-point energy curve (ZPE) as functions of s (amu)$^{1/2}$ bohr for the reactions

R1a and R1b. Note that the $V_a^G = V_{MEP} + ZPE$. From Figure S1a, it is seen that the plots of the V_a^G and V_{MEP} are similar in shape and locations, the curves of V_a^G and V_{MEP} have the same zenith in the position direction s = 0 (amu) $^{1/2}$ bohr, indicating that the variational effect will be small in the calculation of the rate constant for the channel R1a. This will be borne out in the following study. For Reaction R1b, Figure S1b shows that the maximum of V_a^G and V_{MEP} is located at the saddle point (s = 0). However, the curve of V_a^G differs from the curve of and V_{MEP} in their shape, especially in s = 1.0 (amu) $^{1/2}$ bohr. The result suggests that the variational effect might be important in evaluating the rate constant. Jia et al.[45] have theoretically studied the reaction C_2H_5I with Cl atom, similar results can be found about potential energy curves in their paper. The following study of the rate constants will support this view deeply.

Figure S2a and S2b show that the variations of the generalized normal-mode vibrational frequencies along with the MEPs for reactions R1a and R1b, respectively. It is obvious that the frequency of mode 1, which connects the stretching vibrational mode of breaking and forming bonds, changes significantly near the saddle point (s = 0). There are 20 generalized vibrational frequencies in the vicinity of the transition state from Figure S2a. The deep minimum in frequency takes place in the range from –0.34 to 0.34 (amu) $^{1/2}$ bohr. In Figure S2b, in the negative limit of s ($s = -\infty$), the frequencies are associated with those of the reactants, and in the product region at about 2.0 (amu) $^{1/2}$ bohr, the frequencies correspond to those of the product complex, EP1b. In the process of the reaction, most of those frequencies also do not change

significantly in going from the reactants to the products, but the frequency of mode 1, has a dramatic drop as the reaction progress. In the vicinity of the transition state, 29 generalized vibrational frequencies were found. The deep minimum in frequency takes place in the range from 0.34 to 0.34 (amu) $^{1/2}$ bohr. It is known to call the significant changes "reaction mode", which is to be the typical behavior of H-transfer reactions.[34,35,45,46] Therefore, it is reasonable for these reactions to perform generalized normal-mode analysis using rectilinear coordinates in the present study.

3.4. Rate constant calculations and branching ratios

The dual-level dynamics calculations of the title reaction are carried out at the CCSD(T)/II//B3LYP/I level. The rate constants are evaluated by conventional transition state theory (TST), canonical variational transition state theory (CVT), and the CVT with the small-curvature tunneling (SCT)yue contributions in a wide temperature range from 220 to 800 K. The TST, CVT, and CVT/SCT rate constants of the reactions R1a and R1b are plotted against the reciprocal of temperature in Figure 3a and 3b. The CVT/SCT rate constants of k_{1a}, k_{2a}, k_{3a}, k_{1b}, k_{2b}, k_{3b}, k_{4b} and the corresponding total rate constant k_a ($k_a = k_{1a} + k_{2a} + k_{3a}$), k_b ($k_b = k_{1b} + k_{2b} + k_{3b} + k_{4b}$), along with the experimental values are listed in Table 2a and 2b.

Figure 3a shows that the CVT and TST rate constants for reaction R1a are almost superposed on each other over the whole temperature range, suggesting that the variational effects can be negligible. However, deviations between the CVT and CVT/SCT rate constants are notable over the lower temperature range, implying that

the tunneling contribution plays an important role in calculations of the rate constants at low temperatures. For instance, the ratios of CVT/SCT and CVT rate constants are 2.28×10^2 at 220 K, 24.88 at 298 K, 3.35 at 500 K, and 1.50 at 800 K. This is not the only feature of the present reaction system but also has been found in other similar reaction, as investigated by Jia et al.[45] In addition, it can be seen from Figure 3b that the ratios of CVT rate constant and TST rate constant are 0.22–0.24 in the temperature of 220–800 K, showing that the variational effects should be taken into account in calculations of rate constants of R1b. The tunneling effect was found to be important for reaction R1b in the lower temperatures and unimportant when the temperature is high. For example, the specific values of rate constants between the CVT/SCT and CVT are 49.30, 12.64, 3.15, and 1.65 at 220, 298, 500, and 800 K, respectively. From Table 2a, it is pleasing to observe that the calculated rate constant 2.13×10^{-13} cm^3 $molecule^{-1}$ s^{-1} is in excellent accord with the experimental value,[9,11] 4.10×10^{-13} cm^3 $molecule^{-1}$ s^{-1} for reaction of CH_3I with NO_3 radical at 298 K. For reaction C_2H_5I with NO_3, theoretical overall rate constant, 1.97×10^{-13} cm^3 $molecule^{-1}$ s^{-1} is in commendable agreement with the experimental value, 2.40×10^{-13} cm^3 $molecule^{-1}$ s^{-1}.[12] The above reasonable accordance between the experimental and theoretical data shows that the computed and predicted dynamic information about the title reactions is very credible. The rate constants calculations show that the rate constants for the H-abstraction reaction channels all have positive temperature effect in the temperature range of 220–800 K. The positive temperature effect about the rate constants for reaction $CH_3I + NO_3$ in experimental temperature of 298–323 K is found, which will

support our obtained conclusion about the temperature dependence. Similar theoretical results can be also found in the reaction of C_2H_5I with Cl atom[45] and other alkyl iodides reaction with O(^{3}P) and OH radicals.[19, 47,48]

Figure 4a and 4b show the temperature dependence of branching ratios for the reactions of CH_3I and C_2H_5I with NO_3 radical, respectively. It can be found from Figure 4a that both of the channels R1a and R2a are important in the total reaction and the contribution of pathway R3a can be ignored at the whole temperature range (220–800 K). The contribution of R1a becomes larger with the temperature increasing. However, the contribution of R1b decreases with the temperature increasing. Figure 4b shows that R1b is the main reaction channel in the whole temperature range. Channel R3b contributes more than R2b to the overall reaction constant when the temperature below 350 K, but with the temperature increasing, the contribution of channel R2b should be considered. The influence of displacement channel R4b to the total rate constant can be also neglectful. Thus, for the multichannel reaction of C_2H_5I + NO_3, the dominant channel is the H-abstraction from the –CH_2– group leading to the product CH_3CHI. However, the contribution from the –CH_3 group can not be ignored in the high temperatures.

3.5. Atmospheric photolysis of CH_3I, C_2H_5I, and iodine-containing complexes

As stated above EP1a, EP2a, EP1b, EP2b, and EP3b are very stable formed in the title reactions. It is known that the NO_3 radicals can be easily photolyzed by the sunlight. However, the photolysis of iodine-containing complexes formed in the atmosphere by

NO_3 radical with CH_3I and C_2H_5I is not clear. The photolysis of CH_3I, C_2H_5I, and complexes should be discussed and compared. We calculated the vertical excitation energy (T_V) of the first fifteen excited states for CH_3I, C_2H_5I, EP1a, EP2a, EP1b, EP2b, and EP3b. The same method B3LYP, 6-311++G(d,p) basis set for C, N, O, H atoms and cc-pVTZ-PP for iodine were employed in the calculations. Calculated results are listed in Table S2 and Figure S3.

It is well known that if the T_V value is lower than 4.13 eV (about 300 nm), the compound is considered to undergo photolysis in the sunlight. From the Table S2, it can be seen that the T_V value of CH_3I and C_2H_5I is higher than 4.13 eV, suggesting that the photolysis of these two species is difficult. However, T_V values of the first five excited states for EP1a, EP2a, EP1b, first six excited states for EP2b, and first seven excited states for EP3b are smaller than 4.13 eV, indicating that these complexes can be photolyzed under sunlight. The oscillator strength of fourth exited state from EP1a, EP2a, and EP1b are 0.055, 0.0475, and 0.0569, implying that strong photolysis happened at about 328, 331, and 326 nm, respectively. As for EP2b and EP3b, the T_V value and oscillator strength third exited state are 3.4077, 3.3507 eV and 0.2093, 0.1272 at about 363 and 370 nm, respectively. We can speculate that the ability of photolysis of complexes is larger than CH_3I and C_2H_5I. Once the complexes are generated, the stable complexes might be photolyzed as the source of iodine-containing compounds in the atmosphere.

3.6. Atmospheric lifetime of CH_3I and C_2H_5I at nighttime

Due to the NO_3 average concentrations at nighttime is very high than other radicals, thus, the nighttime tropospheric lifetime (τ) of CH_3I and C_2H_5I can be estimated by assuming that its removal from troposphere occurs only through the reactions with NO_3 radical. The expression can be shown as, $\tau_{NO3} = k_{NO3}([NO_3])^{-1}$. Using the total rate constants 1.81×10^{-13} cm^3 $molecule^{-1}$ s^{-1} for reaction $CH_3I + NO_3$ and 9.22×10^{-14} cm^3 $molecule^{-1}$ s^{-1} for reaction $C_2H_5I + NO_3$ at 270 K and the global atmospheric NO_3 concentrations[15,16] of 5×10^8 molecule cm^{-3}. The lifetime of CH_3I and C_2H_5I is estimated to be 3.07 h and 5.86 h, which is in good agreement with the experimental values 3.0 h and 5.0 h,[9,12] respectively. The short lifetime indicates that the reactions of CH_3I and C_2H_5I with NO_3 will play important roles in the formation of the reactive iodine compounds.

3.7. NO_3 radical initiated oxidation of CH_3I and C_2H_5I

The mechanism and oxidation pathways of CH_3I and C_2H_5I in a NO_3-rich environment to form the IO radical and aldehydes is displayed in Figure 5. The subsequent reactions of title reactions can produce iodine monoxide radical (IO), formaldehyde, and acetaldehyde. Iodine monoxide radical is a class of reactive iodine compound, which plays an important role in the iodine cycle in the atmosphere of Earth. It can involve in the ozone depleting cycle to affect the oxidation capacity of the atmosphere.[9,11,12] Due to the source of IO radical mainly from the sunlight photolysis of alkyl iodides, it has been considered to be inexistent in the marine boundary layer at nighttime until Saiz-Lopez et al. [49] observed an important nighttime concentration. The

aldehydes are the important VOCs, which have the potential adverse health effects on humans and play crucial roles in atmospheric photochemical reactions.[50] The reaction of CH_3I with NO_3 will go through mainly via H-abstraction leads to the CH_2I radical. Then the CH_2I radical reaction with O_2 mainly leads to the formaldehyde and IO radical with a relatively fast rate constant of $(4.0 \pm 0.4) \times 10^{-13}$ cm^3 $molecule^{-1}$ s^{-1}. In fact, once CH_2I radical is formed in the atmosphere, CH_2I may also reaction with other species such as NO_2 and more. In 2010, we have already studied the detailed reaction mechanism on the radical–radical reaction of $CH_2I + NO_2$, two primary products P1 ($CH_2O + INO$), P2 ($CHIO + HNO$) and one secondary product P3 ($CH_2O + I + NO$) observed.[3] For the NO_3 radical initiated oxidation of C_2H_5I, one pathway is CH_3CHI formed by the H-abstraction of NO_3 radical from the $–CH_2–$ group. And then the CH_3CHI can reaction with O_2 to produce acetaldehyde and IO radical. For the reaction mechanism of $CH_3CHI + NO_2$, we will investigate it in the future. Another pathway is H-abstraction of NO_3 radical from the $–CH_3$ group, and it leads to the formation of CH_2CH_2I, which is unstable and may release I atom and ethylene. The emitted I atoms in the atmosphere will be inclined to react with O_3 to form the IO radicals. Therefore, the subsequent reactions of CH_3I/C_2H_5I with NO_3 radicals may be important for formation of IO radical and aldehydes.

Because of the lacking of the experimental data in other temperature range, the three-parameter Arrhennius fits based on the calculated rate constants at the CCSD(T)/I//B3LYP/I level within 220–800 K give expressions as follows (in units of cm^3 $molecule^{-1}$ s^{-1}):

$k_{1a}(T)=1.28\times10^{-32}T^{6.86}\exp(1231.95/T)$

$k_{2a}(T)=4.87\times10^{-31}T^{6.30}\exp(1295.90/T)$

$k_{3a}(T)=7.92\times10^{-24}T^{4.02}\exp(-7142.51/T)$

$k_{1b}(T)=4.95\times10^{-22}T^{4.08}\exp(-1032.73/T)$

$k_{2b}(T)=1.20\times10^{-23}T^{4.60}\exp(-1741.94/T)$

$k_{3b}(T)=1.42\times10^{-20}T^{3.92}\exp(-2866.61/T)$

$k_{4b}(T)=1.25\times10^{-23}T^{5.20}\exp(-9125.76/T)$

$k_{a}(T)=8.62\times10^{-32}T^{6.66}\exp(1324.23/T)$

$k_{b}(T)=9.48\times10^{-27}T^{5.75}\exp(-655.34/T)$

4. Conclusions

In this article, reactions of $CH_3I + NO_3$ and $C_2H_5I + NO_3$ are investigated in kinetics by the dual-level direct method. The potential energy surface information is obtained at the B3LYP level with 6-311++G(d,p) basis set for C, H, O, N, and cc-pVTZ-PP basis set for iodine atom. The higher level energies for the stationary points are refined at the QCISD(T) and CCSD(T) levels same basis set for C, H, O, N, and aug-cc-pVTZ-PP basis set for iodine atom. The rate constants of all the H-abstraction reactions are calculated by CVT incorporating SCT correction. The agreement between theoretical and experiment result is very excellent. In the temperature range of 220–800 K, the variational effect is almost negligible for R1a and important for R1b. The tunneling effect is significant in the whole temperature range. All the five H-abstractions rate constants are positive temperature coefficients. Our results show

that two H-abstraction channels are both important for reaction $CH_3I + NO_3$. For reaction of $C_2H_5I + NO_3$, R1b is the main reaction pathway, and the role of R2b and R3b can not be ignored in high temperatures. Additionally, the lifetime for CH_3I and C_2H_5I computed using the rate coefficients is obtained to be 3.03 and 5.86 h, respectively. The short lifetime of them may result from the release of iodine by reaction with active radicals. The three-parameter Arrhenius expressions for the title reactions are $k_a = 8.62 \times 10^{-32} T^{6.66} \exp(1324.23/T)$, $k_b = 9.48 \times 10^{-27} T^{5.75} \exp(-655.34/T)$ cm^3 molecule^{-1} s^{-1}. We hope our theoretical studies may provide a good estimate for further laboratory understanding the title reactions.

Acknowledgments

The authors thank Professor Donald G. Truhlar for providing the Polyrate, Version 9.7 program. This work is supported by National Natural Science Foundation of China (No. 21377021), and Fund of Jilin Provincial Science & Technology Department (No. 20120401).

References

1 A. Saiz-Lopez, J. M. C. Plane, A. R. Baker, L. J. Carpenter, R. Von Glasow, J. C. Gómez Martín, G. McFiggans, R. W. Saunders, *Chem. Rev*. 2012, **112**, 1773–1804.
2 S. L. Zhang, R. S. Strekowski, A. Monod, L. Bosland, and C. Zetzsch, *J. Phys. Chem. A* 2012, **116**, 9497–9506.
3 X. J. Jia, Y. J. Liu, J. Y. Sun, H. Sun, F. Wang, Z. M. Su, X. M. Pan, R. S. Wang, *Theor. Chem. Acc*. 2010, **127**, 49–56.
4 S. Klick, K. Abrahamsson, *J. Geophys. Res*. 1992, **97**, 12683–12687.
5 C. Schall, K. G. Heumann, *Fresen. J. Anal. Chem*. 1993, **346**, 717–722.
6 L. J. Carpenter, W. T. Sturges, S. A. Penkett, P. S. Liss, B. Alicke, K. Hebestreit, U. Platt, *J. Geophys. Res*. 1999, **104**, 1679–1689.

7 E. S. N. Cotter, C. E. Canosa-Mas, C. R. Manners, R. P. Wayne, D. E. Shallcross, *Atmos*. *Environ*. 2003, **37**, 1125–1133.
8 C. E. Jones, K. E. Hornsby, R. M. Dunk, R. J. Leigh, L. J. Carpenter, *Atmos*. *Chem*. *Phys*. 2009, **9**, 8757−8769.
9 Y. Nakano, and T. Ishiwata, M. Kawasaki, *J*. *Phys*. *Chem*. *A* 2005, **109**, 6527-6531.
10 Y. Nakano, H. Ukeguchi, T. Ishiwata, *Chem*. *Phys*. *Lett*. 2006, **430**, 235-239.
11 Y. Nakano, H. Ukeguchi, T. Ishiwata, Y. Kanaya, H. Tachikawa, A. Ikeda, S. Sakaki, and M. Kawasaki, *Bull*. *Chem*. *Soc*. *Jap*. 2008, **81**, 938–946.
12 Y. Nakano, Y. Hoshob, K. Sadamori, T. Ishiwata, *Chem. Phys*. *Lett*. 2012, **535**, 26–29.
13 F. Karagulian, M. J. Rossi, *Phys*. *Chem. Chem*. *Phys*. 2005, **7**, 3150−3162.
14 R. Kamens, D. Bell, A. Dietrich, J. Perry, R. Goodman, L. Claxton, S. Tejada, *Environ*. *Sci*. *Technol*. 1985, **19**, 63−69.
15 T. E. Kleindienst, P. B. Shepson, E. O. Edney, L. D. Claxton, L. T. Cupitt, *Environ*. *Sci*. *Technol*. 1986, **20**, 493−501.
16 M. Ezzati, D. M. Kammen, *Environ*. *Heal*. *Persp*. 2002, **110**, 1057−1068.
17 G. Bravo-Pérez, J. R. Alvarez-Idaboy, A. Cruz-Torres, M. E. Ruíz, *J*. *Phys*. *Chem*. *A* 2002, **106**, 4645−4650.
18 M. T. Rayez, J. C. Rayez, I. Kerdouci, and B. Picquet-Varrault, *J*. *Phys*. *Chem. A* 2014, **118**, 5149−5155.
19 S. L. Zhang, R. Strekowski, A. Monod, L. Bosland, C. Zetzsch, *Int*. *J*. *Chem*. *Kinet*. 2014, **46**, 554–566.
20 J. R. Alvarez-Idaboy, A. Galano, G. Bravo-Peréz, M. E. Ruiz, *J*. *Am. Chem*. *Soc*. 2001, **123**, 8387−8395.
21 C. G. Liu, P. Zhang, Y. F. Wang, B. Yang, and J. Shu, *Environ*. *Sci*. *Technol*. 2012, **46**, 13262−13269.
22 A. Moreno, S. Salgado, R. Taccone, P. Martín, B. Cabanas, *Atmos*. *Environ*. 2014, **96**, 229−235.
23 M. J. Frisch, G. W. Trucks, H. B. Schlegel, P. W. M. Gill, B. G. Johnson, M. A. Robb, J. R. Cheeseman, T. A. Keith, G. A. Petersson, J. A. Pople, et al., 2009. Gaussian 09. Gaussian Inc., Wallingford, CT.
24 A. D. Becke, *J*. *Chem*. *Phys*. 1993, **98**, 1372–1377.
25 C. Lee, W. Yang, R. G. Parr, *Phys*. *Rev*. *B* 1998**, 37**, 785–789.
26 K. A. Peterson, C. Puzzarini, *Theor*. *Chem*. *Acc*. 2005, **114**, 283−296.
27 Y. Z. Tang, Y. R. Pan, J. Y. Sun, R. S. Wang, *Chem*. *Phys*. 2008, **344**, 221–226.
28 X. W. Fan, X. H. Ju, *J*. *Comput*. *Chem*. 2008, **29**, 505–513.
29 C. Gonzalez, H. B. Schlegel, *J*. *Chem*. *Phys.* 1989, **90**, 2154−2161.
30 C. Gonzalez, H. B. Schlegel, *J*. *Chem*. *Phys*. 1990, **94**, 5523−5527.
31 K. Raghavachari, G. W. Trucks, J. A. Pople, M. A. Head-Gordon, *Chem*. *Phys*. *Lett*. 1989, **157**, 479−483.
32 J. A. People, M. A. Head-Gordon, K. Raghavachari, *J*. *Chem*. *Phys*. 1989, **87**, 5968−5975.
33 K. A. Peterson, D. Figgen, E. Goll, H. Stoll, M. Dolg, *J*. *Chem*. *Phys*. 2003, **119**, 11113–11123.

34 F. Y. Bai, G. Sun, X. Wang, Y. Q. Sun, R. S. Wang, X. M. Pan, *J. Phys. Chem. A* 2015, **119**, 1256−1266.
35 F. Y. Bai, X. L. Zhu, Z. M. Jia, X. Wang, Y. Q. Sun, R. S. Wang, X. M. Pan, *ChemPhysChem*. 2015, **16**, 1768−1776.
36 B. C. Garrett, D. G. Truhlar, *J. Chem. Phys*. 1979, **70**, 1593−1598.
37 B. C. Garrett, D. G. Truhlar, *J. Am. Chem. Soc*. 1979, **101**, 4534−4548.
38 B. C. Garrett, D. G. Truhlar, R. S. Grev, A. W. Magnuson, *J. Phys. Chem*. 1980, **84**, 1730−1748.
39 D. H. Lu, T. N. Truong, V. S. Melissas, G. C. Lynch, Y. P. Liu, B. C. Grarrett, R. Steckler, A. D. Issacson, S. N. Rai, G. C. Hancock, J. G. Lauderdale, T. Joseph, D. G. Truhlar, *Comput. Phys. Commun*. 1992, **71**, 235−262.
40 Y. P. Liu, G. C. Lynch, T. N. Truong, D. H. Lu, D. G. Truhlar, B. C. Garrett, *J. Am. Chem. Soc*. 1993, **115**, 2408−2415.
41 Y. Y. Chuang, J. C. Corchado, D. G. Truhlar, *J. Phys. Chem. A* 1999, **103**, 1140−1149.
42 J. C. Corchado, Y. Y. Chuang, P. L. Fast, W. P. Hu, Y. P. Liu, G. C. Lynch, K. A. Nguyen, C. F. Jackels, A. Fernandez-Ramos, B. A. Ellingson, et al. POLYRATE, version 9.7; University of Minnesota: Minneapolis, MN, 2007.
43 I. S. Ignatyev, Y. M. Xie, W. D. Allen, H. F. Schaefer, *J. Chem. Phys*. 1997, **107**, 141−155.
44 H. B. Schlegel, C. Sosa, *Chem. Phys. Lett*. 1988, **145**, 329−333.
45 X. J. Jia, Y. J. Liu, J. Y. Sun, H. Sun, F. Wang, Z. M. Su, X. M. Pan, R. S. Wang, *J. Comput. Chem*. 2010, **31**, 2263–2272.
46 F. Y. Bai, Y. Q. Sun, X. Wang, Z. M. Jia, R. S. Wang, X. M. Pan, *J. Mol. Model*. 2014, **20**, 2419.
47 M. A. Teruel, T. J. Dillon, A. Horowitz and J. N. Crowley. *Phys. Chem. Chem. Phys*. 2004, **6**, 2172–2178.
48 M. Sudolska, F. Louis, and I. Cernusak, *J. Phys. Chem. A* 2014, **118**, 9512–9520.
49 A. Saiz-Lopez, J. M. C. Plane, *Geophys. Res. Lett*. 2004, **31**, L04112.
50 Y. M. Ji, Y. P. Gao, G. Y. Li, T. C. An, *Atmos. Environ*. 2012, **54**, 288−295.

Table 1. Relative energies (*E*r) of main species, Reaction enthalpies ($\Delta H^{\theta}_{r,298}$) and reaction Gibbs

free energies ($\Delta G^{\theta}_{r,298}$) for reactions R1a—R4b at the B3LYP/I, CCSD(T)/II//B3LYP/I, and QCISD(T)/II//B3LYP/I levels (kcal/mol) with the ZPE (in Hartree) or TZPE (thermal corrections to enthalpy) corrections..

Species	ZPE(B3LYP)	B3LYP	CCSD(T)//B3LYP	QCISD(T)//B3LYP
*E*r				
CH_3I+NO_3	0.047175	0.00	0.00	0.00
TS1a	0.045643	6.52	10.54	10.72
EP1a	0.049714	0.03	-3.43	-2.89
TS2a	0.045557	7.00	10.33	10.46
EP2a	0.049727	0.61	-2.97	-2.45
CH_2I+HNO_3	0.047773	1.79	-0.70	-0.11
TS3a	0.050111	17.41	23.00	23.69
EP3a	0.054231	-16.42	-19.49	-18.87
CH_3NO_3+I	0.054001	-16.27	-18.44	-17.80
$C_2H_5I+NO_3$	0.075911	0.00	0.00	0.00
TS1b	0.073913	3.38	7.15	7.29
EP1b	0.078413	-3.85	-7.28	-6.73
$CH_3CHI+HNO_3$	0.076951	-1.06	-2.71	-1.03
TS2b	0.074261	4.94	9.58	9.71
EP2b	0.078825	-9.57	-10.80	-10.08
TS3b	0.073425	8.75	10.41	10.65
EP3b	0.078751	-13.04	-14.01	-13.29
$CH_2CH_2I+HNO_3$	0.077909	-8.41	-7.83	-6.04
TS4b	0.078303	15.25	23.02	23.17
EP4b	0.082557	-20.10	-23.98	-21.65
$CH_3CH_2NO_3+I$	0.082292	-18.91	-20.95	-20.32
$\Delta H^{\theta}_{r,298}$				
R1a (R2a)		1.91	-0.58	0.01
R3a		-16.65	-18.82	-18.19
R1b		-1.02	-2.67	-0.99
R2b(R3b)		-8.11	-7.53	-5.75
R4b		-19.16	-21.20	-20.57
$\Delta G^{\theta}_{r,298}$				
R1a (R2a)		1.84	-0.65	-0.07
R3a		-12.05	-14.22	-13.58
R1b		-1.13	-2.77	-1.10
R2b(R3b)		-9.48	-8.90	-7.11
R4b		-14.54	-15.59	-15.95

Table 2a. Calculated CVT/SCT rate constants (cm^3 $molecule^{-1}$ s^{-1}) along with the experimental

values (Italics) for reactions of NO_3 radical with CH_3I in the temperature range of 220–800 K.

T(K)	k_{1a}	k_{2a}	k_{3a}	k_a
220	4.96×10^{-14}	1.19×10^{-13}	1.82×10^{-27}	1.69×10^{-13}
270	6.07×10^{-14}	1.20×10^{-13}	5.44×10^{-25}	1.81×10^{-13}
296	7.37×10^{-14}	1.36×10^{-13}	5.75×10^{-24}	2.10×10^{-13}
298	7.49×10^{-14}	1.38×10^{-13}	6.80×10^{-24}	2.13×10^{-13}
				$(4.10\pm0.10)\times10^{-13}$[a,b]
303	7.81×10^{-14}	1.42×10^{-13}	1.03×10^{-23}	2.20×10^{-13}
				$(4.20\pm0.60)\times10^{-13}$[a]
313	8.51×10^{-14}	1.51×10^{-13}	2.26×10^{-23}	2.36×10^{-13}
				$(4.80\pm1.00)\times10^{-13}$[a]
323	9.30×10^{-14}	1.61×10^{-13}	4.78×10^{-23}	2.54×10^{-13}
				$(6.30\pm1.00)\times10^{-13}$[a]
350	1.19×10^{-13}	1.95×10^{-13}	3.02×10^{-22}	3.14×10^{-13}
400	1.93×10^{-13}	2.88×10^{-13}	5.26×10^{-21}	4.81×10^{-13}
500	4.93×10^{-13}	6.35×10^{-13}	3.67×10^{-19}	1.13×10^{-12}
600	1.16×10^{-13}	1.33×10^{-12}	7.66×10^{-18}	2.49×10^{-12}
800	4.97×10^{-13}	4.68×10^{-12}	4.77×10^{-16}	9.65×10^{-12}

[a]Reference[9]
[b]Reference[11]

Table 2b. Calculated CVT/SCT rate constants (cm^3 $molecule^{-1}$ s^{-1}) along with the experimental

values (Italics) for reactions of NO_3 radical with C_2H_5I in the temperature range of 220–800 K.

T(K)	k_{1b}	k_{2b}	k_{3b}	k_{4b}	k_b
220	1.75×10^{-14}	4.37×10^{-16}	9.29×10^{-17}	2.30×10^{-29}	1.80×10^{-14}
270	8.70×10^{-14}	3.65×10^{-15}	1.56×10^{-15}	1.07×10^{-25}	9.22×10^{-14}
296	1.73×10^{-13}	9.11×10^{-15}	5.15×10^{-15}	3.17×10^{-24}	1.87×10^{-13}
298	1.82×10^{-13}	9.73×10^{-15}	5.61×10^{-15}	4.03×10^{-24}	1.97×10^{-13}
					(2.40±0.40)×10^-13c
303	2.06×10^{-13}	1.14×10^{-14}	6.92×10^{-15}	7.24×10^{-24}	2.24×10^{-13}
313	2.60×10^{-13}	1.57×10^{-14}	1.04×10^{-14}	2.22×10^{-23}	2.86×10^{-13}
323	3.27×10^{-13}	2.12×10^{-14}	1.53×10^{-14}	6.42×10^{-23}	3.64×10^{-13}
350	5.75×10^{-13}	4.50×10^{-14}	3.97×10^{-14}	8.59×10^{-22}	6.60×10^{-13}
400	1.43×10^{-12}	1.50×10^{-13}	1.74×10^{-13}	4.57×10^{-20}	1.75×10^{-12}
500	5.96×10^{-12}	9.84×10^{-13}	1.71×10^{-12}	1.49×10^{-17}	8.65×10^{-12}
600	1.77×10^{-11}	4.08×10^{-12}	9.09×10^{-12}	8.41×10^{-16}	3.09×10^{-11}
800	8.80×10^{-11}	3.17×10^{-11}	9.26×10^{-11}	1.68×10^{-13}	2.12×10^{-10}

[c]Reference[12]

Figure captions

Figure 1. Optimized geometries of the reactants, products, transition states, and complexes at the B3LYP/I level. Bond lengths are in angstroms and angles in degrees.

Figure 2. Schematic potential energy surface (a) for reaction $CH_3I + NO_3$ and (b) for reaction $C_2H_5I + NO_3$. Relative energies (in kcal/mol) are calculated at the CCSD(T)/II//B3LYP/I + ZPE level).

Figure 3. Calculated TST, CVT, and CVT/SCT rate constants as a function of $10^3/T$ for reaction channels R1a (a), and R1b (b) in the temperature range of 220–800 K.

Figure 4. Calculated branching ratios as a function of $10^3/T$ for reactions $CH_3I + NO_3$ (a), and $C_2H_5I + NO_3$ (b) at the CCSD(T)/II//B3LYP/I level.

Figure 5. NO_3 radical initiated atmospheric degradation mechanism for CH_3I and C_2H_5I.

(a)

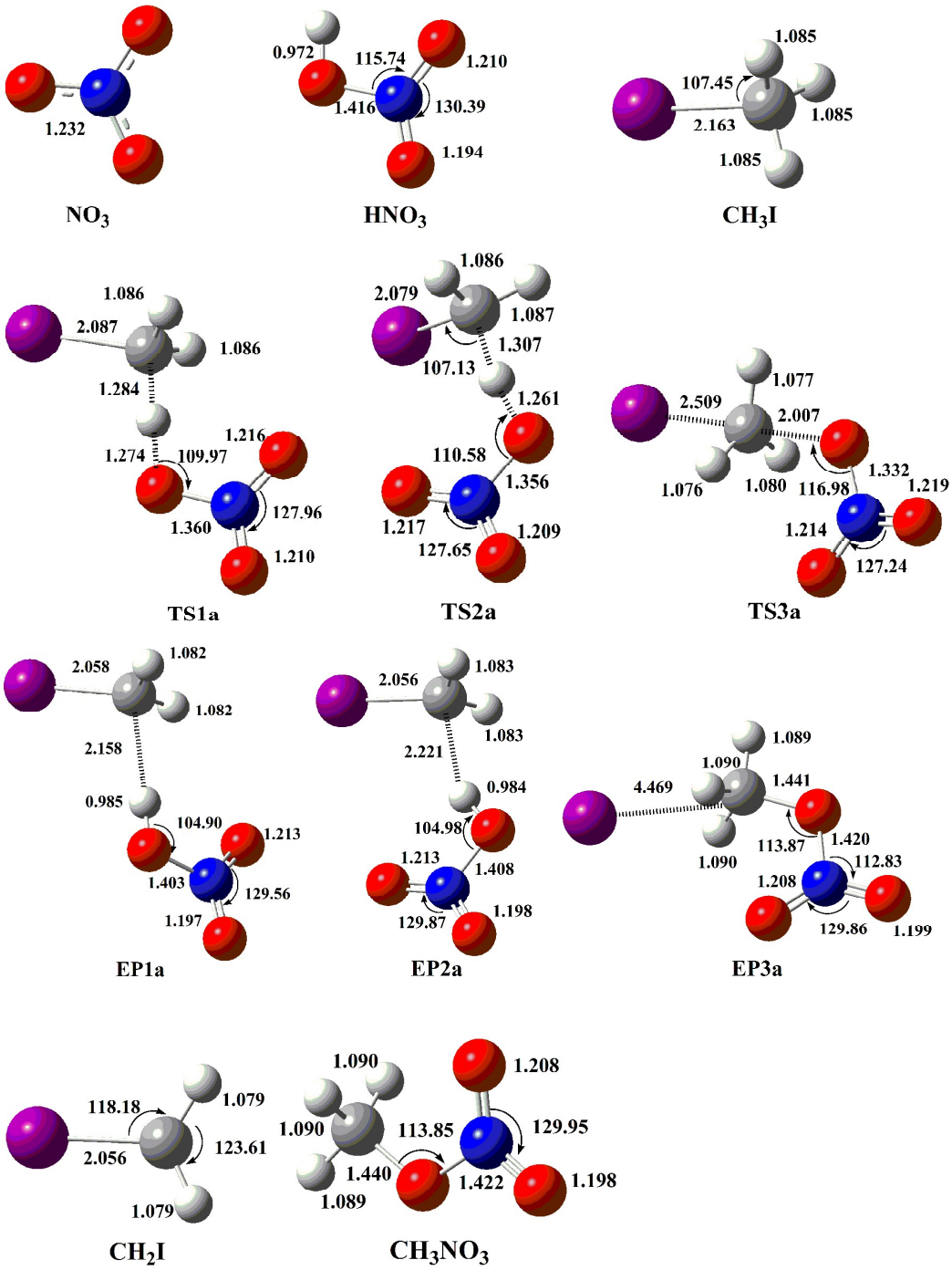

Figure 1

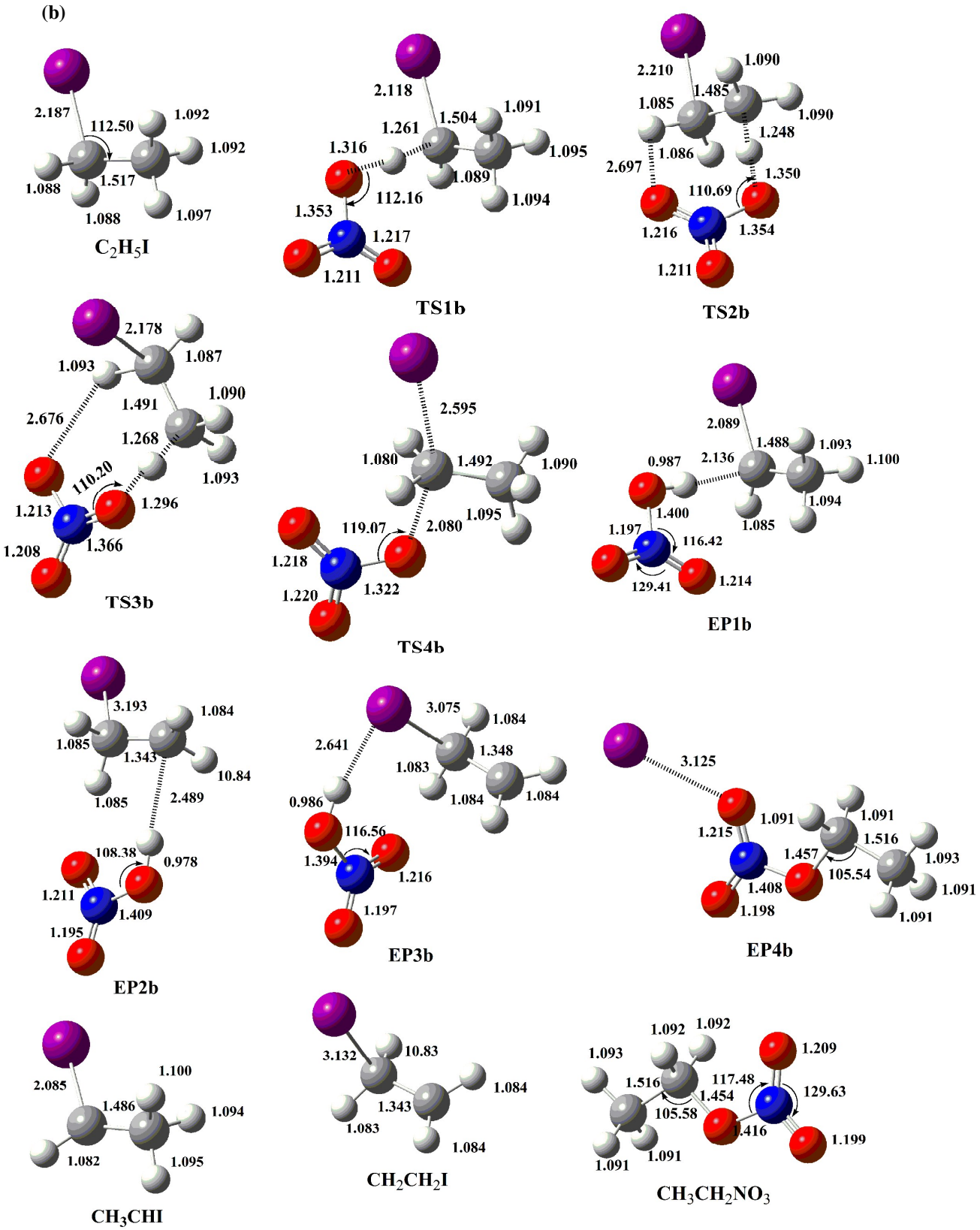

Figure 1 (*continued*)

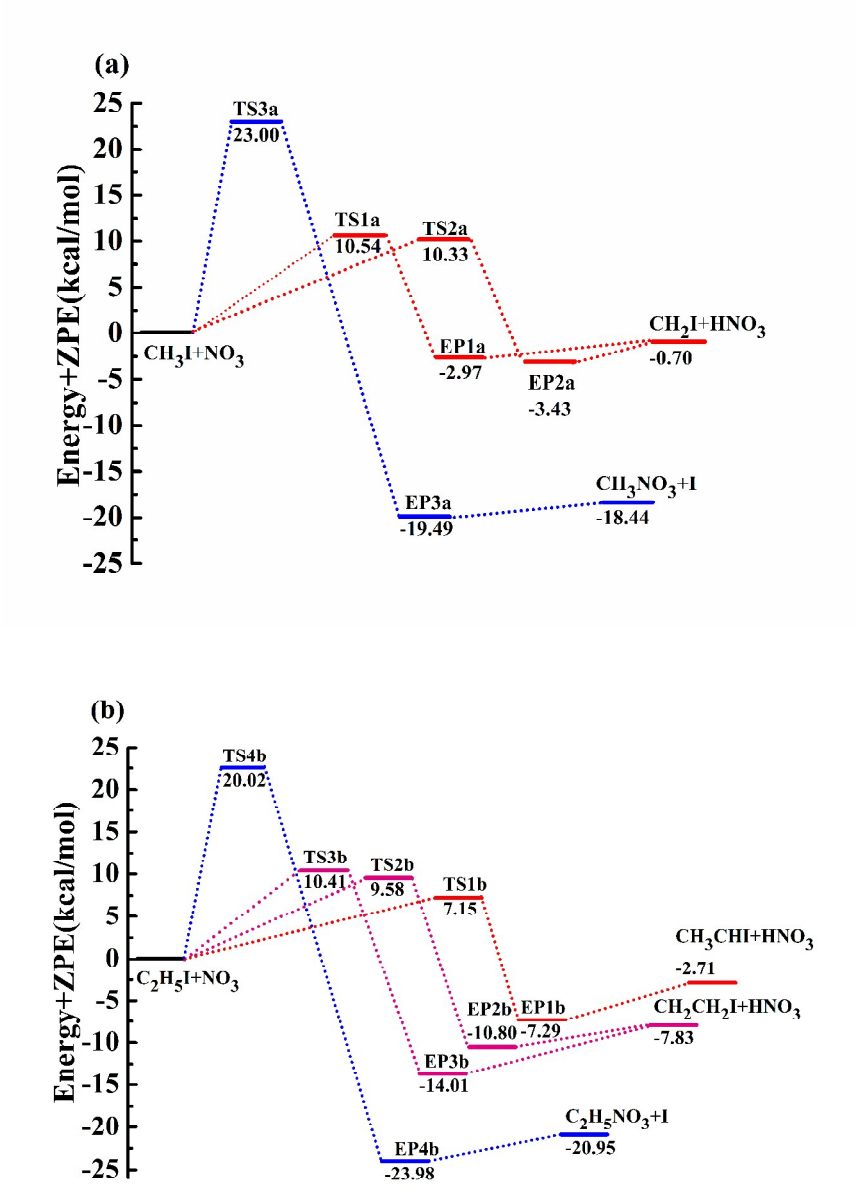

Figure 2

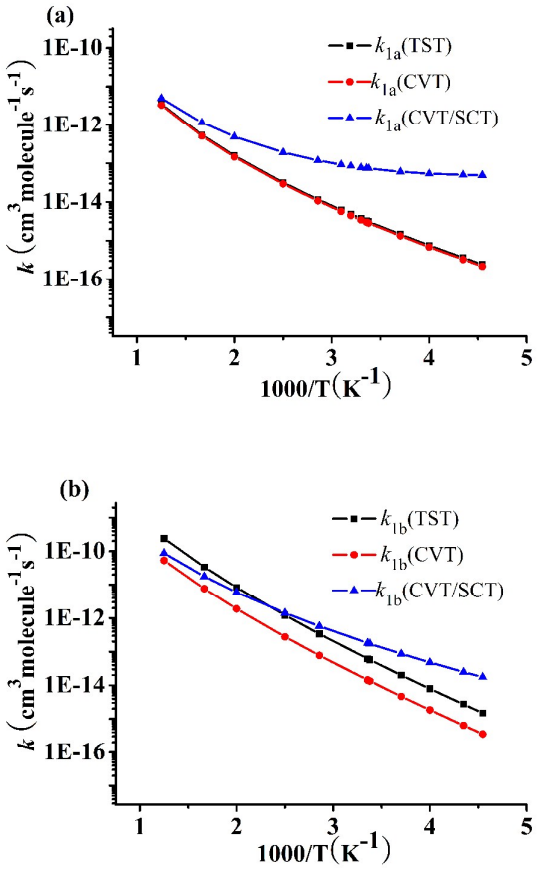

Figure 3

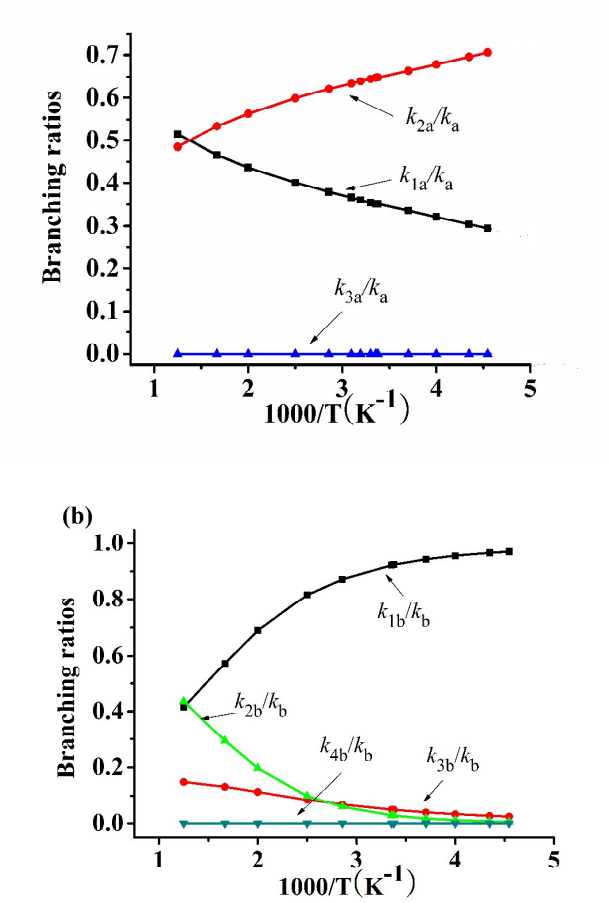

Figure 4

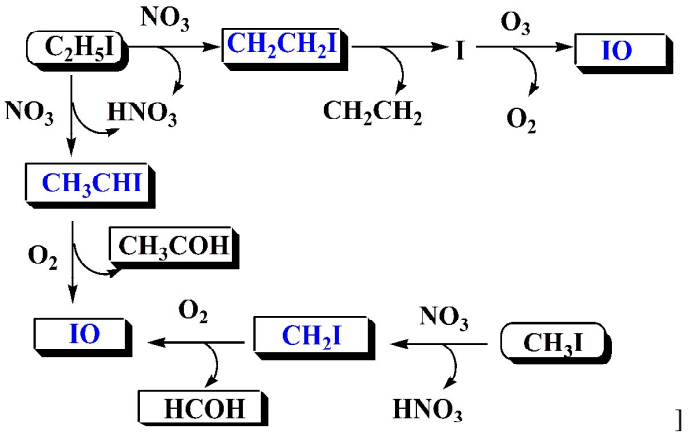

]

Figure 5

Highlights

Mechanisms and kinetics of the reactions of NO_3 radical with CH_3I and C_2H_5I have been investigated on a sound theoretical basis.

Graphic